European Journal of Immunology

Innate immunity

Basic

Research Article

Hobit and Blimp-1 instruct the differentiation of iNKT cells into resident-phenotype lymphocytes after lineage commitment

Natasja AM Kragten[#1], *Renske LRE Taggenbrock*[#1], *Loreto Parga Vidal*[1], *Rene AW van Lier*[1], *Regina Stark*[‡1,2] *and Klaas PJM van Gisbergen*[‡1,2]

[1] Dept. of Hematopoiesis, Sanquin Research and Landsteiner Laboratory Amsterdam UMC, Amsterdam, The Netherlands

[2] Dept. of Experimental Immunology, Amsterdam UMC, Amsterdam, The Netherlands

iNKT cells are CD1d-restricted T cells that play a pro-inflammatory or regulatory role in infectious and autoimmune diseases. Thymic precursors of iNKT cells eventually develop into distinct iNKT1, iNKT2, and iNKT17 lineages in the periphery. It remains unclear whether iNKT cells retain developmental potential after lineage commitment. iNKT cells acquire a similar phenotype as tissue-resident memory T cells, suggesting that they also differentiate along a trajectory that enables them to persist in peripheral tissues. Here, we addressed whether lineage commitment and memory differentiation are parallel or sequential developmental programs of iNKT cells. We defined three subsets of peripheral iNKT cells using CD62L and CD69 expression that separate central, effector, and resident memory phenotype cells. The majority of iNKT1 cells displayed a resident phenotype in contrast to iNKT2 and iNKT17 cells. The transcription factor Hobit, which is upregulated in iNKT cells, plays an essential role in their development together with its homolog Blimp-1. Hobit and Blimp-1 instructed the differentiation of central memory iNKT cells into resident memory iNKT cells, but did not impact commitment into iNKT1, iNKT2, or iNKT17 lineages. Thus, we conclude that memory differentiation and the establishment of residency occur after lineage commitment through a Hobit and Blimp-1-driven transcriptional program.

Keywords: Blimp-1 · Differentiation · Hobit · iNKT cells · Lineage commitment · Tissue residency

Additional supporting information may be found online in the Supporting Information section at the end of the article.

Introduction

Invariant NK T (iNKT) cells are innate-like T cells that possess a semi-invariant T cell receptor (TCR) and recognize glycolipids presented by the non-polymorphic MHC molecule CD1d. iNKT cells are situated in different locations of the body, with the highest frequencies detected in liver, thymus, and spleen. At these locations, iNKT cells contribute to tissue homeostasis by rapidly

Correspondence: Natasja AM Kragten; Klaas PJM van Gisbergen
e-mail: n.kragten@sanquin.nl; k.vangisbergen@sanquin.nl

[#]Contributed equally as first author.
[‡]Contributed equally as senior author.

secreting cytokines and cytotoxic molecules upon activation via cognate antigen, danger signals, or pro-inflammatory cytokines such as IL-12 and type I IFN. iNKT cells mediate tumor surveillance [1, 2] and can play a protective role in infection, but their pro-inflammatory activity can also trigger immunopathology in autoimmune diseases.

iNKT cells are generated in the thymus, where the selection and specification of iNKT cells are driven by the recognition of CD1d molecules on other thymocytes [3]. In contrast to conventional T cells, which migrate as naive T cells from the thymus, iNKT cells already acquire memory characteristics in the thymus, as evidenced by the upregulation of the memory-associated molecule CD44. Functional heterogeneity exists within the mature iNKT cell population of the thymus and the periphery and three major populations are recognized [4]. iNKT1 cells upregulate the transcription factor T-bet and mainly produce IFN-γ after stimulation. iNKT2 and iNKT17 cells secrete IL-4 and IL-17, respectively, instructed by the transcription factors GATA3 in iNKT2 and RORγt in iNKT17 [4]. However, it is not clear whether lineage specification instructed by these transcription factors also drives terminal differentiation of the three iNKT lineages or whether additional maturation steps occur after lineage commitment of iNKT cells.

iNKT cells are largely maintained as non-circulatory cells that permanently reside in the thymus, spleen, or liver under steady-state conditions [5–7]. We have previously demonstrated that liver iNKT cells show a transcriptional signature of tissue-residency, similar to tissue-resident memory CD8 T cells and other resident innate lymphocytes [8]. Parabiosis experiments have demonstrated that the vast majority of liver iNKT cells are not exchanged between parabionts [9, 10]. In contrast, iNKT cells in other organs such as in lymph nodes appear to display heterogeneity in respect to residency [7,9,11]. The expression of the C-type lectin CD69 has been strongly associated with residency in memory CD8 T cells [12]. Similarly, $CD69^+$ iNKT cells demonstrate a higher degree of tissue residency compared to $CD69^-$ iNKT cells [7, 11]. These findings suggest that iNKT cells with different migration and homing potential can be identified through CD69 expression. Currently, it remains unclear whether lineage commitment and memory differentiation resulting in the establishment of tissue residency represent sequential or parallel transcriptional programs in iNKT cells.

Here, we report that CD69 and CD62L delineate tissue-resident memory T cell (TRM), effector memory T cell (TEM), and central memory T cell (TCM) subsets in iNKT cells. The prevalence of TRM-phenotype cells was substantially higher in the iNKT1 lineage compared to the iNKT2 and iNKT17 lineages, which were associated with higher expression of the transcription factor Hobit. We have previously reported that the transcription factors Hobit and its homolog Blimp-1 drive the tissue-residency program of innate and adaptive immune cells including that of iNKT cells [8]. Here, we observed that Hobit and Blimp instructed the differentiation of TRM-phenotype cells at the expense of TEM and TCM phenotype cells, but did not impact specification in iNKT1, iNKT2, and iNKT17 lineages. Our findings show that Hobit and Blimp-1 drive a transcriptional program of tissue residency after lineage commitment of iNKT cells. Thus, iNKT1, iNKT2, and iNKT17 cells retain potential to branch out into iNKT subsets resembling TRM, TEM, and TCM cells, which is under the control of Hobit and Blimp-1.

Results

CD69 and CD62L identify iNKT cell subsets with resident and circulating phenotypes

iNKT cells are largely maintained as tissue-resident cells in the liver and spleen [9,13]. Consistent with these observations, analysis of the expression of the residency-associated molecule CD69 and the lymph node homing receptor CD62L on iNKT cells showed that the majority of iNKT cells in the thymus, spleen, and liver displayed a resident ($CD69^+CD62L^-$) phenotype (Figure 1A and B; Supporting Information Figure S1A). Minor populations of iNKT cells with an effector memory ($CD69^-CD62L^-$) phenotype and a central memory ($CD69^-CD62L^+$) phenotype were present in the thymus, spleen, and liver (Figure 1A and B). In contrast, iNKT cells within the brachial and mesenteric lymph nodes contained a large fraction of central memory phenotype cells (Figure 1A and B). It should be noted that CD69 does not provide absolute demarcation between resident and effector memory phenotype iNKT cells in these tissues. Below, we will designate the populations of iNKT cells that were identified by CD69 and CD62L expression as $iNKT_{RM}$ ($CD69^+CD62L^-$), $iNKT_{EM}$ ($CD69^-CD62L^-$), and $iNKT_{CM}$ ($CD69^-CD62L^+$). Residency-associated molecules such as CD39, CD49a, CXCR6, and P2RX7 [14] were nearly uniformly expressed in $iNKT_{RM}$ cells (Figure 1C and D). In contrast, these molecules were nearly absent or low in $iNKT_{EM}$ and $iNKT_{CM}$ cells (Figure 1C and D). Furthermore, the transcription factor TCF7 and the lymph node homing molecule CCR7 that strongly associate with circulating T cells were nearly absent from $iNKT_{RM}$, but expressed in a substantial fraction of $iNKT_{EM}$ and $iNKT_{CM}$ (Figure 1C and D). These data demonstrate that CD62L and CD69 accurately identify subsets of iNKT cells with a resident memory, effector memory, and central memory phenotype.

Hobit is upregulated in $iNKT_{TRM}$ cells

We previously found that Hobit expression identifies lymphocytes with a resident phenotype such as tissue-resident memory $CD8^+$ T cells (T_{RM}) and ILC1 [8]. Therefore, we investigated whether Hobit expression is associated with iNKT cells displaying a resident phenotype using our recently developed Hobit reporter mice that contain tdTomato, Cre recombinase, and diphtheria toxin under the control of the endogenous Hobit promotor [15]. To assess whether tdTomato faithfully reported Hobit expression in iNKT cells, we analyzed the expression of tdTomato in iNKT cells of WT and Hobit reporter mice. Expression of tdTomato was observed in a large fraction of thymic iNKT cells of Hobit reporter mice, but not in thymic iNKT cells of WT mice (Figure 2A and

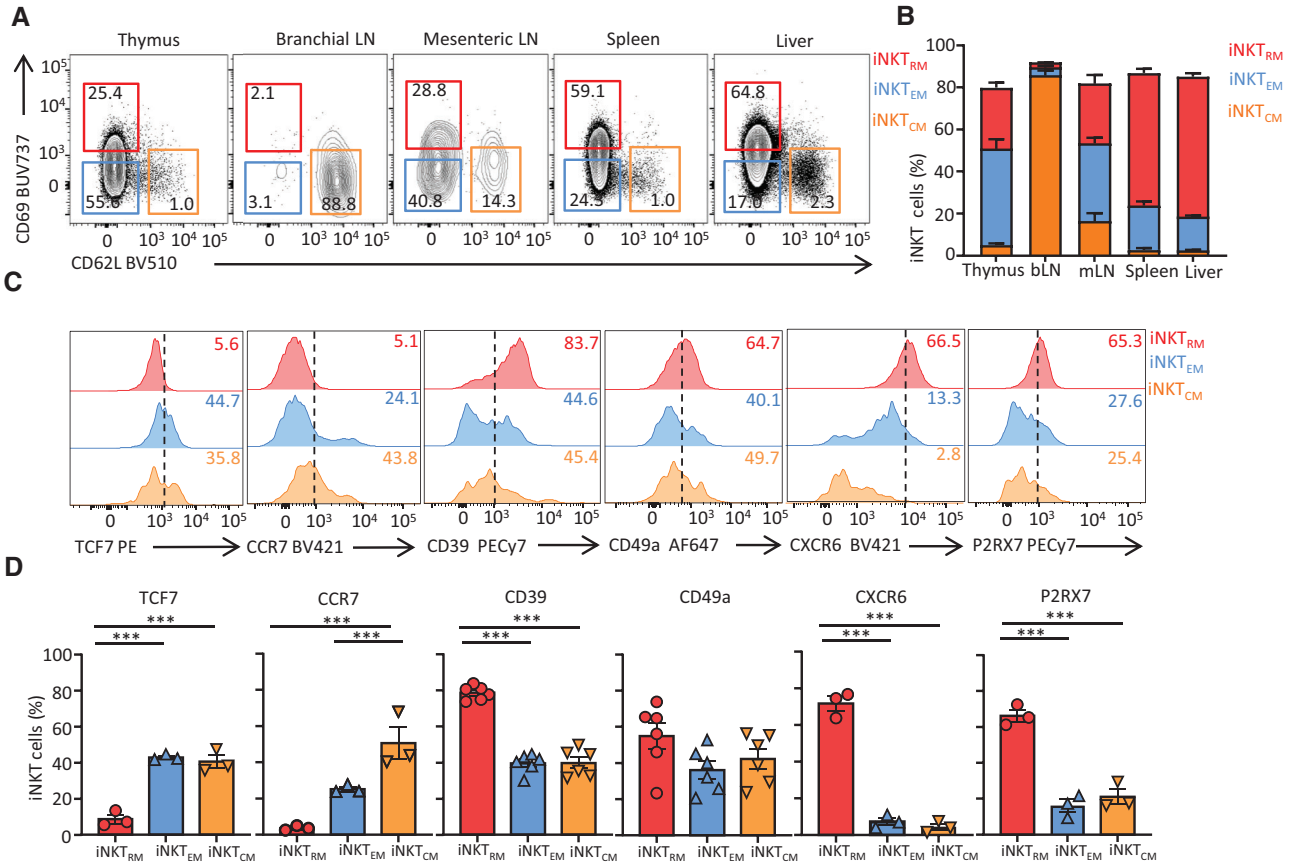

Figure 1. The majority of iNKT cells display a resident phenotype. The expression of CD69, CD62L, and TdTomato was analyzed in PBS57-CD1d tetramer$^+$ iNKT of Hobit reporter mice using flow cytometry. (A) Contour plots depict CD69 and CD62L expression on iNKT cells in the indicated tissues to identify iNKT$_{RM}$ (CD69$^+$CD62L$^-$, red), iNKT$_{EM}$ (CD69$^-$ CD62L$^-$, blue) and iNKT$_{CM}$ (CD69$^-$ CD62L$^+$, orange). (B) The graph shows the percentage of iNKT$_{RM}$ (red), iNKT$_{EM}$ (blue), and iNKT$_{CM}$ (orange) within the iNKT population of the indicated organs. (C) Histograms depict the expression of TCF7, CCR7, CD39, CD49a, CXCR6, and P2RX7 in splenic iNKT$_{RM}$ (red), iNKT$_{EM}$ (blue), and iNKT$_{CM}$ (orange). (D) Graphs display the frequency of TCF7, CCR7, CD39, CD49a, CXCR6, and P2RX7 expression in splenic iNKT$_{RM}$ (red), iNKT$_{EM}$ (blue), and iNKT$_{CM}$ (orange). Plots in (A) and (C) are representative of data shown in (B) and (D), respectively. The graph in B displays data from 3 mice per group and is representative for at least 3 independent experiments. The graphs in (D) display data from three to six mice and are representative of at least two independent experiments. Symbols represent individual mice, error bars SEM. One-way ANOVA, $^{***}p < 0.0005$.

B). We have previously reported that thymic Ly49C/I$^+$ iNKT cells are dependent on Hobit in contrast to other thymic and peripheral iNKT cells [16]. The formation of thymic iNKT cell subsets including Ly49C/I$^+$ iNKT cells was comparable between WT and Hobit reporter mice, suggesting that the reporter insert did not impact NKT cell differentiation (Supporting Information Figure S1B and C). We observed that tdTomato expression was upregulated during differentiation of iNKT cells at stage 2 and maintained in mature thymic Ly49C/I$^-$ and Ly49C/I$^+$ iNKT cells (Supporting Information Figure S1D and E). Peripheral iNKT cell populations in the spleen and liver largely expressed tdTomato in contrast to iNKT cells in lymph nodes including those in brachial and mesenteric lymph nodes (Figure 2C and D). In contrast to thymic CCR7$^-$ iNKT cells, Hobit was not present in thymic CCR7$^+$ iNKT cells, which have been shown to represent a late precursor stage that emigrates from the thymus to seed peripheral iNKT populations (Supporting Information Figure S2A and B) [17]. These findings suggest that Hobit expression is separately acquired during iNKT cell maturation in the thymus and in the periphery. Furthermore, tdTomato (Hobit) expression was not present in DN, DP, CD4$^+$ SP, and CD8$^+$ SP thymocytes (Supporting Information Figure S3A-C) and also not in mature splenic CD4$^+$ T cell subsets including naive, central memory, and effector memory CD4$^+$ T cells (Supporting Information Figure S3D-F). Taken together, these results show that the Hobit reporter enables visualization and characterization of iNKT cell differentiation.

To address whether Hobit identified subsets of circulating and resident iNKT cells, we determined the expression of molecules associated with tissue residency in Hobit$^-$ and Hobit$^+$ fractions of iNKT cells. We observed that the Hobit$^+$ fraction of iNKT cells nearly uniformly expressed the residency-associated molecules CD39, CD49a, CD69, CXCR6, and P2RX7 (Figure 2E and F). These residency-associated molecules were only expressed in a minor proportion of Hobit$^-$ iNKT cells (Figure 2E and F). In contrast, expression of CD62L and CCR7, which associate with central memory phenotype T cells, was present within the Hobit$^-$ fraction of iNKT cells, but was nearly absent from the Hobit$^+$ fraction of iNKT cells (Figure 2E and F). Vice versa, Hobit

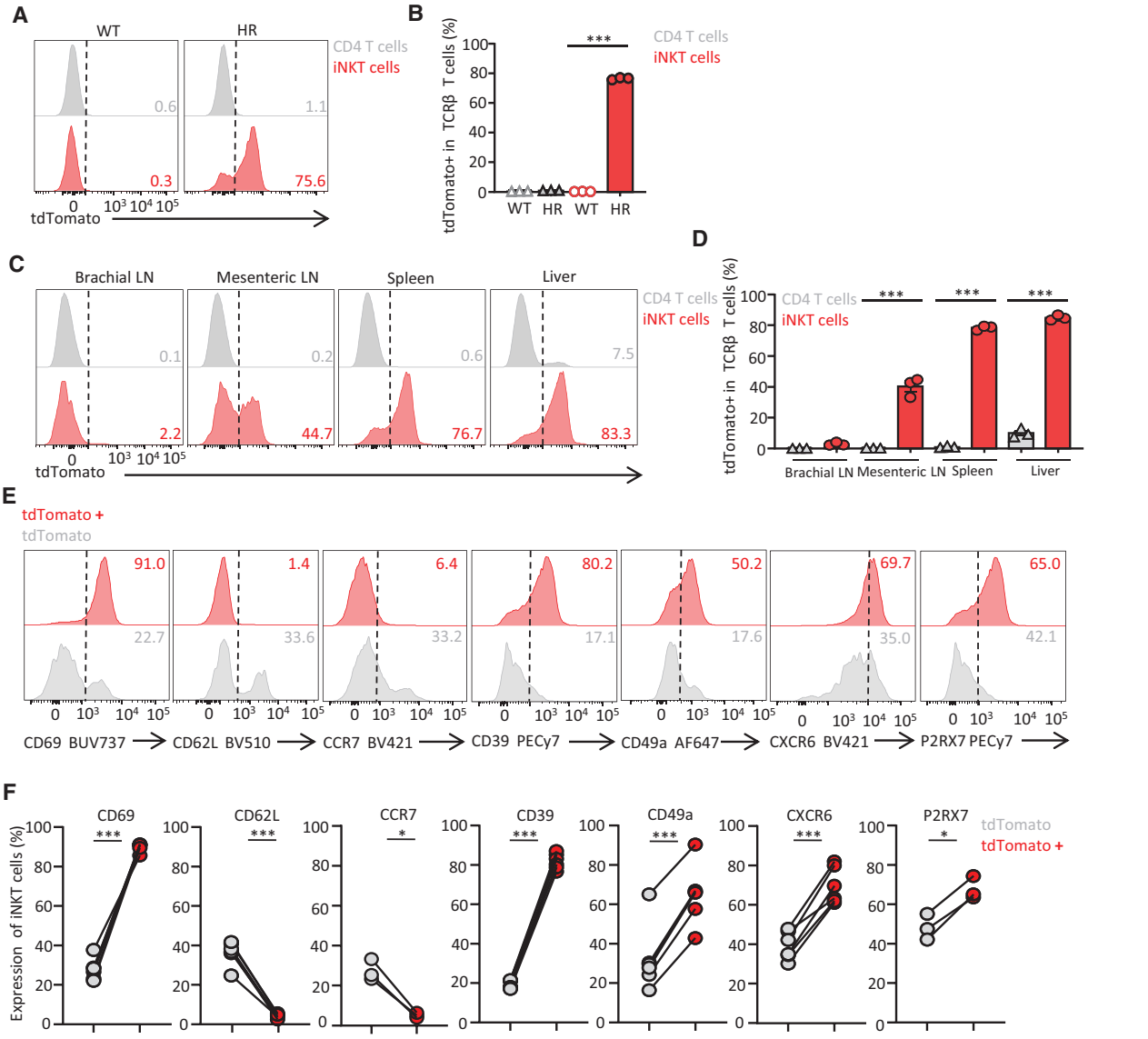

Figure 2. Hobit is expressed in iNKT cells under steady-state conditions. The expression of Hobit (tdTomato) was analyzed in PBS57-CD1d tetramer$^+$ specific iNKT cells using flow cytometry. (A) Histograms display tdTomato expression in thymic iNKT cells (red) and CD4 T cells (grey) in WT and Hobit reporter mice. (B) The graph displays the frequency of tdTomato expression in thymic iNKT cells (red) and CD4 T cells (grey) of WT and Hobit reporter mice. (C) Histograms depict tdTomato expression in iNKT cells (red) and CD4 T cells (grey) of brachial LN, mesenteric LN, spleen, and liver of Hobit reporter mice. (D) The graph displays the frequency of tdTomato expression in iNKT cells (red) and CD4 T cells (grey) of Hobit reporter mice within the indicated tissues. (E) Histograms display the expression of CD69, CD62L, CCR7, CD39, CD49a, CXCR6, and P2RX7 in splenic tdTomato$^-$ (grey) and tdTomato$^+$ iNKT cells (red) of Hobit reporter mice. (F) Graphs display the frequency of CD69, CD62L, CCR7, CD39, CD49a, CXCR6, and P2RX7 expression on splenic tdTomato$^-$ (grey) and tdTomato$^+$ (red) iNKT cells of Hobit reporter mice. Plots in (A), (C), and (E) are representative of data shown in (B), (D), and (F), respectively. The graph in (B) displays data from three mice per group and are representative for at least three independent experiments. Graphs in (D) and (F) display data of three to six mice and are representative of at least two experiments. Symbols represent individual mice, error bars SEM. One-way ANOVA, or paired *T*-Test, $^*p < 0.05$, $^{***}p < 0.0005$.

expression was present in nearly the complete fraction of iNKT$_{RM}$ cells and in a fraction of iNKT$_{EM}$ cells, but the transcription factor was largely absent from iNKT$_{CM}$ cells (Supporting Information Figure S4A and B). The Hobit-related transcription factor Blimp-1 collaborates with Hobit in the regulation of tissue-resident lymphocytes [8]. To investigate the co-expression of Hobit and Blimp-1 in iNKT cells, we employed Hobit mice that simultaneously reported Hobit and Blimp-1 expression through tdTomato and GFP, respectively. We observed strong co-expression of Blimp-1 and Hobit in iNKT$_{RM}$ and in a fraction of iNKT$_{EM}$ (Supporting Information Figure S5A and B). In contrast, Hobit and Blimp-1 expression were largely absent from iNKT$_{CM}$ (Supporting Information Figure S5A and B). These data demonstrate that Hobit and Blimp-1 mainly characterize iNKT cells with a resident memory phenotype in a similar fashion as other tissue residency-associated molecules.

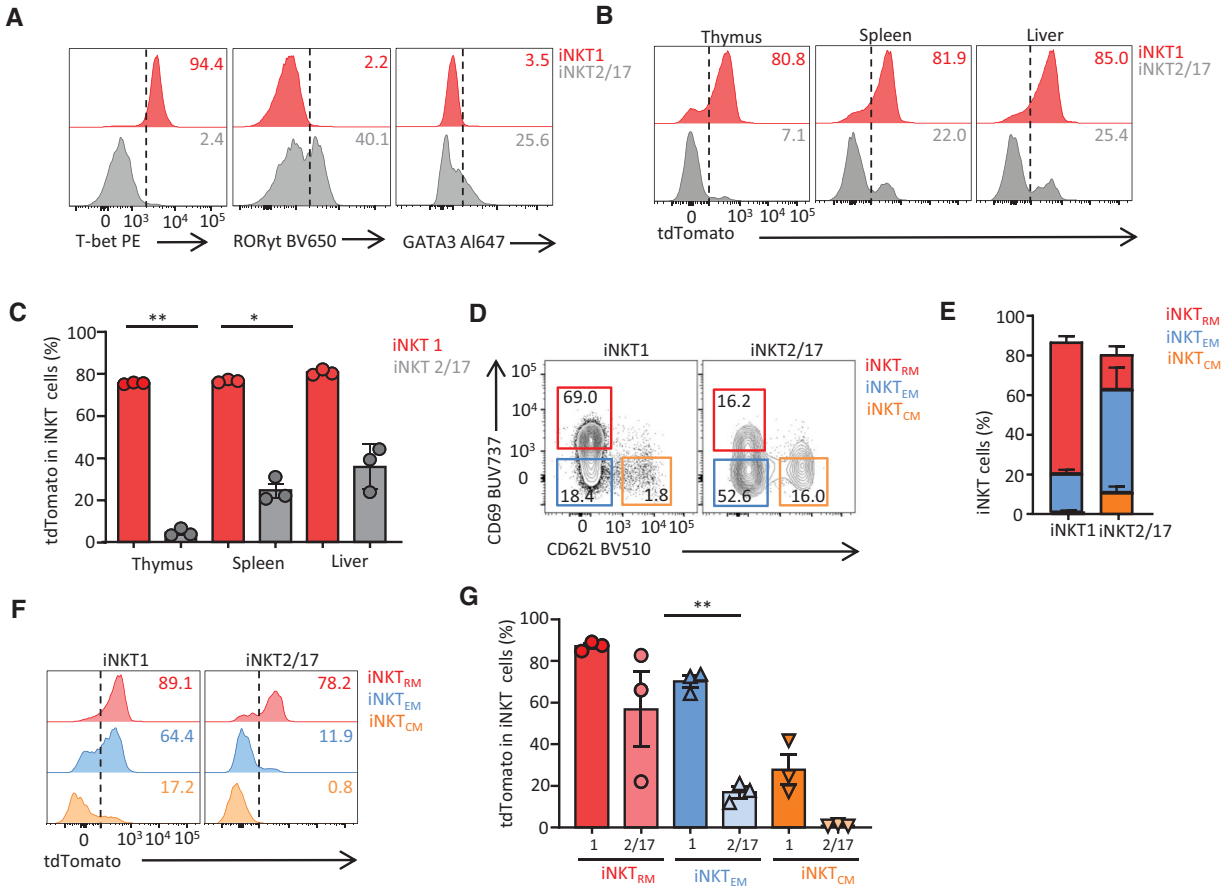

Figure 3. Hobit expression is largely restricted to iNKT1 and iNKT2/17 cells with a resident phenotype. The expression of Hobit (tdTomato) in PBS57-CD1d tetramer$^+$ CD122$^+$ iNKT1 cells and CD122$^-$ iNKT2/17 cells was analyzed in Hobit reporter mice using flow cytometry. (A) The histogram displays the expression of the transcription factors T-bet (left), RORγt (center), and GATA3 (right) in iNKT1 (red) and iNKT2/17 (grey) in the thymus. (B) The histogram displays the expression of tdTomato in iNKT1 (red) and iNKT2/17 (grey) of the indicated organs. (C) The graph displays the frequency of tdTomato expression in iNKT1 (red) and iNKT2/17 (grey) of the indicated organs. (D) Contour plots display the frequency of CD69 and CD62L expression on splenic iNKT1 cells (left) and iNKT2/17 cells (right). (E) The graph displays the frequency of iNKT$_{RM}$ (red), iNKT$_{EM}$ (blue), and iNKT$_{CM}$ (orange) within the iNKT1 and iNKT2/17 subsets of the spleen. (F) Histograms depict the expression of tdTomato in splenic iNKT$_{RM}$ (red), iNKT$_{EM}$ (blue), and iNKT$_{CM}$ (orange) fractions of iNKT1 (left) and iNKT2/17 (right). (G) The graph displays the frequency of tdTomato expression in iNKT$_{RM}$ (red), iNKT$_{EM}$ (blue), and iNKT$_{CM}$ (orange) fractions of the iNKT1 and iNKT2/17 populations. Plots in (B), (D), and (F) are representative of graphs shown in (C), (E), and (G), respectively. Graphs in (C), (E), and (G) display data from three mice and are representative of at least two independent experiments. Symbols represent individual mice, error bars SEM. One-way ANOVA, $^*p < 0.05$; $^{**}p < 0.005$.

Hobit expression is restricted to resident memory phenotype iNKT1 and iNKT2/17 cells

In parallel to the separation of conventional CD4 T cells in Th1, Th2, and Th17 lineages, mature iNKT cells have been previously classified into iNKT1, iNKT2, and iNKT17 subsets. [4]. To address Hobit expression in these iNKT cell subsets, we analyzed for the expression of tdTomato using Hobit reporter mice. To identify iNKT1, we made use of the IL-15 receptor β (CD122), which is specifically expressed on iNKT1 cells [4]. In line with previous studies [4], we observed that the iNKT1-associated transcription factor T-bet was exclusively expressed in CD122$^+$ iNKT cells, whereas the iNKT2 associated transcription factor GATA3 and the iNKT17-associated transcription factor RorγT were restricted to CD122$^-$ iNKT cells (Figure 3A). We found that the majority of CD122$^+$ iNKT1 cells in the thymus, spleen, and liver expressed Hobit in contrast to the CD122$^-$ iNKT2 and iNKT17 populations in these organs, which contained a minor fraction of Hobit$^+$ cells (Figure 3B and C). Analysis of CD69 and CD62L expression on splenic iNKT cells indicated that the majority of iNKT1 cells had a resident phenotype, whereas iNKT2 and iNKT17 cells mainly consisted of cells with an effector memory or central memory phenotype (Figure 3D and E). Strikingly, Hobit expression was mainly observed in the iNKT$_{RM}$ and iNKT$_{EM}$ fraction of the iNKT1 lineage and in the iNKT$_{RM}$ fraction of the iNKT2 and iNKT17 lineage (Figure 3F and G). Thus, Hobit is preferentially expressed in iNKT cells with a resident phenotype, independent of their iNKT1, iNKT2, or iNKT17 classification. The more dominant expression of Hobit in the iNKT1 lineage compared to the iNKT2 and iNKT17 lineages appear to relate to their elevated propensity to acquire a resident memory phenotype.

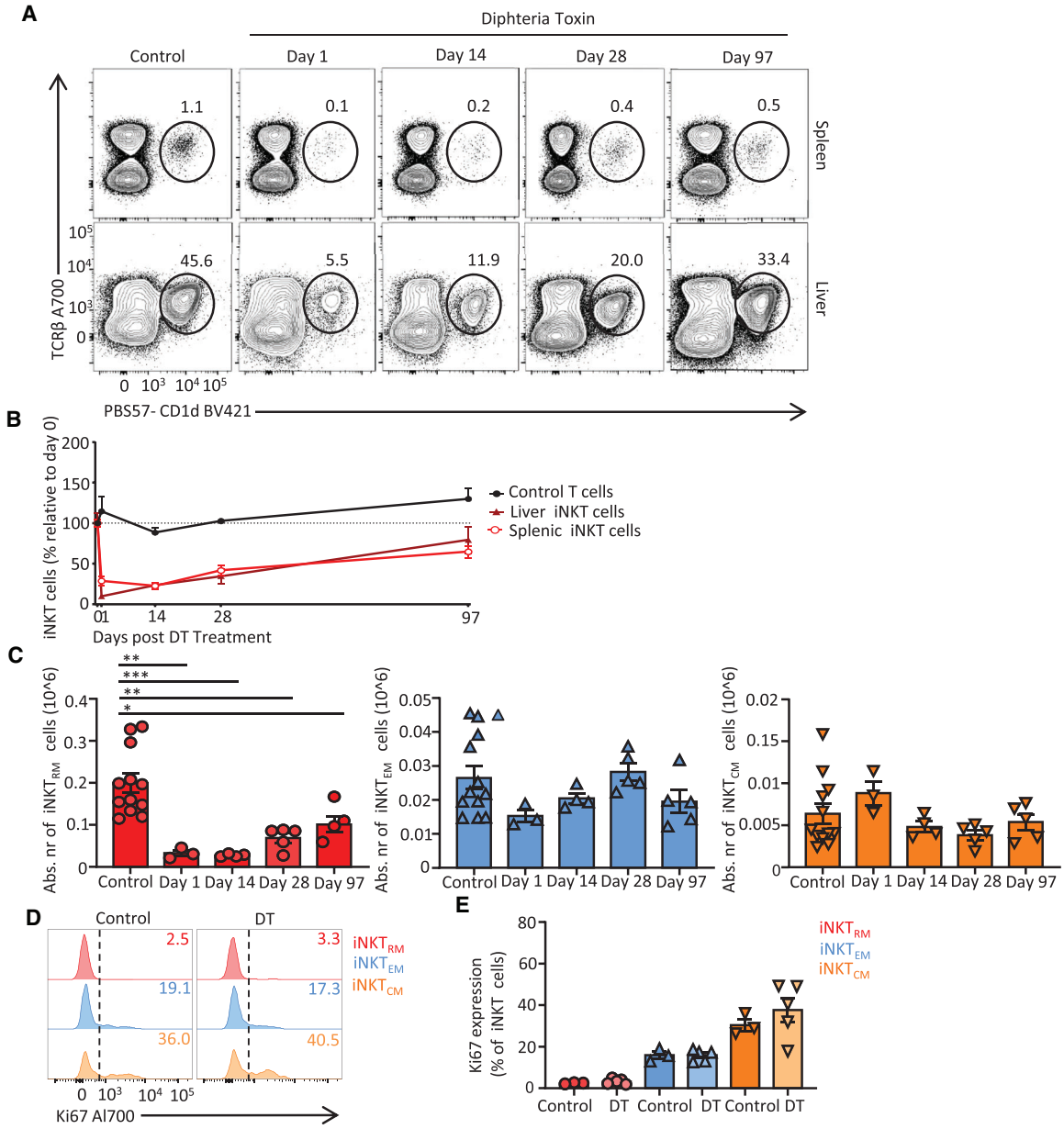

Figure 4. iNKT cells slowly recover after depletion. Hobit$^+$ iNKT cells were deleted in Hobit reporter mice using diphtheria toxin (DT). (A) Contour plots depict the expression of TCRβ and the binding of PBS57-CD1d tetramers to identify iNKT cells in the spleen (upper panels) and liver (lower panels) of control mice and DT treated mice at day 1, 14, 28, and 97 after DT treatment. (B) The graph shows the percentage of iNKT cells and splenic T cells relative to day 0 set at 100% in the indicated organs after DT treatment. (C) Graphs show the absolute number of iNKT$_{RM}$ (left graph, red), iNKT$_{EM}$ (center graph, blue), and iNKT$_{CM}$ (right graph, orange) in the spleen of control and DT treated mice at the indicated days after DT treatment. (D) Histograms show the expression of the proliferation-associated molecule Ki67 in splenic iNKT$_{RM}$ (red), iNKT$_{EM}$ (blue), and iNKT$_{CM}$ (orange) of control mice (left panel) and DT-treated mice at day 14 after DT treatment (right panel). (E) The graph shows the frequency of Ki67 expression in iNKT$_{RM}$ (red), iNKT$_{EM}$ (blue), and iNKT$_{CM}$ (orange) in the spleen of control mice and DT-treated mice at day 14 after DT treatment. Plots in (A) and (D) are representative of data shown in (B) and (E), respectively. Graphs in (B) and (E) display data from 3 to 12 mice per group and are representative of at least two independent experiments. The graph in (E) displays data from three to five mice per group and is representative of two experiments. Symbols represent individual mice, error bars SEM. One-way ANOVA, $^*p < 0.05$; $^{**}p < 0.005$; $^{***}p < 0.0005$.

Hobit$^+$ iNKT cells repopulate under steady-state conditions

Previously, it has been shown that iNKT cell populations are maintained independently of thymic output [18]. To address the maintenance of Hobit$^+$ iNKT cells, we made use of the Hobit-driven diphtheria toxin receptor (DTR), which enables specific deletion of the Hobit$^+$ fraction of iNKT cells. Peripheral iNKT cells were effectively deleted from the thymus, spleen, and liver of Hobit reporter mice directly after treatment with DT

(Figure 4A and B; Supporting Information Figure S6A and B). As expected, the administration of DT resulted in the disappearance of Hobit$^+$ iNKT cells, but not of Hobit$^-$ iNKT cells (Supporting Information Figures S6C and D, and S7A and B). Monitoring of the recovery of iNKT cells over time revealed that iNKT cells steadily repopulated in the thymus, spleen, and liver, but did not fully re-establish the original population within 100 days after DT treatment (Figure 4A and B; Supporting Information Figure S6A and B). Repopulating iNKT cells in DT-treated mice re-expressed Hobit to a similar extent as iNKT cells in control mice that did not receive DT (Supporting Information Figures S6C and D, and S7A and B). These findings suggest that the maintenance of Hobit$^+$ iNKT cells requires local or thymic Hobit$^-$ iNKT cells. However, it remains possible that residual Hobit$^+$ iNKT cells remaining after DT treatment re-establish the population.

Given that Hobit$^-$ iNKT cells mainly consist of iNKT$_{CM}$ and iNKT$_{EM}$ and Hobit$^+$ cells are largely iNKT$_{RM}$, we addressed the dynamics of these subsets after DT treatment. As expected, iNKT$_{RM}$ cells in contrast to iNKT$_{CM}$ and iNKT$_{EM}$ cells were largely depleted in DT-treated Hobit reporter mice (Figure 4C). iNKT$_{CM}$ and iNKT$_{EM}$ populations were stably maintained in the spleen after DT depletion and splenic iNKT$_{RM}$ gradually repopulated over time, but did not reach the size of the original iNKT$_{RM}$ population within 100 days after DT treatment (Figure 4C). The repopulation of iNKT$_{RM}$ cells after DT-driven depletion suggests that iNKT$_{CM}$ or iNKT$_{EM}$ cells contribute to the maintenance of the iNKT$_{RM}$ population. In support, staining of iNKT cells for the proliferation-associated molecule Ki67 showed that iNKT$_{RM}$ contained a minor fraction of Ki67$^+$ cells compared to iNKT$_{EM}$ and iNKT$_{CM}$ in the thymus, spleen, and liver (Figure 4D and E; Supporting Information Figure S8A and B). The DT treatment did not substantially impact the expression of Ki67 in the iNKT subsets (Figure 4D and E), suggesting that iNKT$_{RM}$ were not triggered to replenish the population after DT-driven depletion. Thus, iNKT$_{RM}$ appear to form an inert population of iNKT cells that requires replenishment from other iNKT populations such as iNKT$_{CM}$ and iNKT$_{EM}$ for their long-term maintenance.

Hobit and Blimp-1 do not impact lineage specification into iNKT1, iNKT2, or iNKT17 cells

To address the effect of Hobit and Blimp-1 on iNKT cell differentiation, we made use of Hobit and Blimp-1 deficient mice containing a Hobit reporter. These mice provide a unique opportunity to track the fate of tdTomato$^+$ iNKT cells in the absence of Hobit and Blimp-1. Hobit deficient mice were generated through disruption of the Hobit gene with trapping construct on one allele [16] and with the reporter insert on the other allele. Blimp-1 was specifically deleted using Hobit-driven CRE recombinase to excise the floxed Blimp-1 gene. It is important to note that in this experimental setup Blimp-1 is exclusively deleted in Hobit$^+$ iNKT cells, which does not permit the study of the potential impact of Blimp-1 in early iNKT development prior to Hobit upregulation. The efficiency of the Hobit-driven Cre to delete Blimp-1 in iNKT cells was determined using PCRs that distinguish the deleted from the non-deleted Blimp-1 locus. The Blimp-1 gene was largely deleted in tdTomato$^+$ iNKT cells, but not in tdTomato$^-$ NK cells from the spleen (Supporting Information Figure S9A and C). Thus, we have developed a mouse model that enables us to study the specific role of Hobit and Blimp-1 in iNKT cell development. To assess whether Hobit and Blimp-1 impacted iNKT cell polarization, we analyzed the role of these transcription factors in the differentiation of the iNKT1, iNKT2, and iNKT17 lineages. iNKT cells largely expressed the iNKT1-associated molecule CD122 in the spleen of both Hobit reporter (referred to as WT from here on) and Hobit and Blimp-1 double deficient mice (Figure 5A). The loss of Hobit and Blimp-1 did not affect the relative frequencies of the minor CD122$^-$ iNKT2 and iNKT17 fractions and the major iNKT1 fraction (Figure 5B). Furthermore, tdTomato expression was not increased in CD122$^-$ iNKT cells of Hobit and Blimp-1 double-deficient mice compared to WT mice (Figure 5C and D), suggesting that in the absence of Hobit and Blimp-1 expression, iNKT1 were not redirected into iNKT2 or iNKT17 lineages. These findings were supported using T-bet, RorγT, and GATA3 to identify the iNKT1, iNKT2, and iNKT17 lineages, respectively, in spleen and thymus (Figure 5E-H; Supporting Information Figure S10A-D). We did not observe differences in the frequencies of T-bet$^+$ iNKT1 cells between WT and Hobit × Blimp-1 deficient mice (Figure 5E and F; Supporting Information Figure S10A and B) or of GATA3$^+$ iNKT2 cells and RorγT$^+$ iNKT17 cells in the T-bet$^-$ fraction of iNKT cells (Figure 5G and H; Supporting Information Figure S10C and D). We observed essentially similar results using mixed bone marrow chimeras containing WT and Hobit × Blimp-1 deficient compartments in a 1:1 ratio. CD122 expression was similar between WT and Hobit × Blimp-1 deficient iNKT cells, suggesting that Hobit and Blimp-1 did not impact the size of the iNKT1, iNKT2, and iNKT17 fractions (Supporting Information Figure S11A and B). Furthermore, tdTomato expression was not increased in the CD122$^-$ iNKT cells of the Hobit and Blimp-1 deficient compartment relative to the WT compartment (Supporting Information Figure S11C and D). These findings indicate that Hobit and Blimp-1 are not involved in the regulation of the branching of the iNKT1, iNKT2, and iNKT17 lineages.

Hobit and Blimp-1 control the branching of iNKT$_{CM}$ and iNKT$_{RM}$ cells

Next, we addressed the impact of Hobit and Blimp-1 on the differentiation of iNKT cells into iNKT$_{CM}$, iNKT$_{EM}$, and iNKT$_{RM}$ subsets. As previously observed [8], the combined loss of Hobit and Blimp-1 reduced the frequency and numbers of iNKT cells in the liver, but not the spleen (Figure 6A and B). Splenic and liver iNKT cells of Hobit and Blimp-1 double deficient mice did not acquire an iNKT$_{RM}$ phenotype as efficiently as their WT counterparts (Figure 6C-E). In contrast, we observed an increase in splenic, but not liver, iNKT$_{CM}$, and iNKT$_{EM}$ in Hobit × Blimp-1 double-deficient mice compared to WT mice (Figure 6C-E). We also observed a decrease in thymic iNKT$_{RM}$ cells of Hobit and

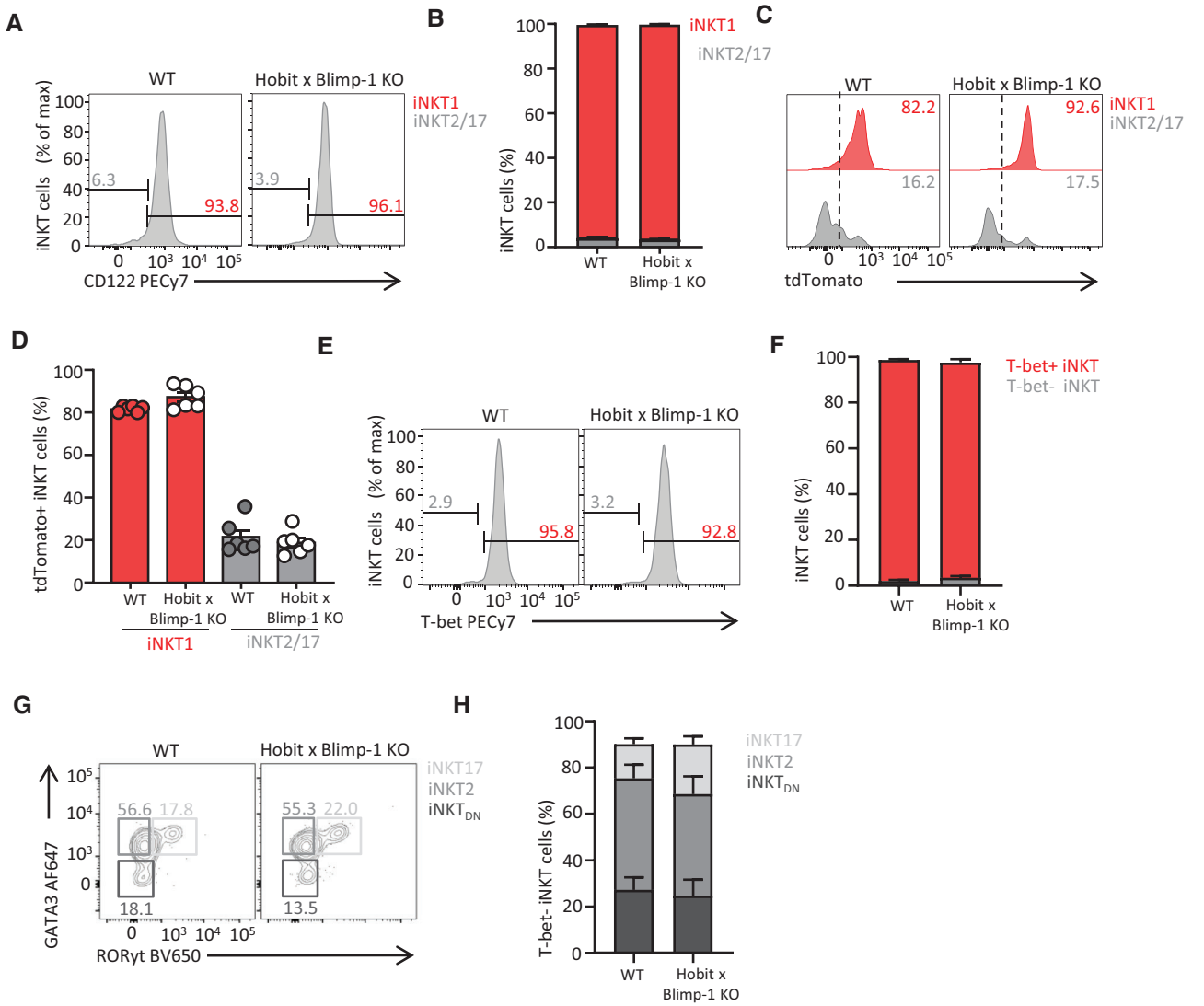

Figure 5. Hobit and Blimp-1 do not regulate differentiation into iNKT1, iNKT2, and iNKT17 lineages. The effect of Hobit and Blimp-1 on the phenotype of iNKT1 and iNKT2/17 cells under steady-state conditions was analyzed in Hobit reporter (WT) and in Hobit and Blimp-1 deficient (Hobit × Blimp-1 KO) mice using flow cytometry. (A) Histograms depict the expression of CD122 on iNKT cells in the spleen of WT and Hobit × Blimp-1 KO mice. (B) The graph displays the frequency of CD122$^-$ iNKT2/17 (grey) cells and CD122$^+$ iNKT1 cells (red) in WT and Hobit × Blimp-1 KO mice. (C) Histograms show the expression of tdTomato in iNKT2/17 (grey) and iNKT1 cells (red) in the spleen of WT and Hobit × Blimp-1 KO mice. (D) The graph displays the frequency of tdTomato expression in splenic iNKT2/17 (grey) and iNKT1 cells (red) of WT and Hobit × Blimp-1 KO mice. (E) Histograms show the expression of T-bet in iNKT cells in the spleen of WT and Hobit × Blimp-1 KO mice. (F) The graph displays the frequency of T-bet- iNKT2/17 cells (grey) and T-bet$^+$ iNKT1 cells (red) in the spleen of WT and Hobit × Blimp-1 KO mice. (G) Contour plots display the expression of GATA3 and RorγT in splenic T-bet$^-$ iNKT cells to identify iNKT$_{DN}$ (GATA3$^-$, RORγt$^-$; black), iNKT2 (GATA3$^+$, RORγt$^-$; dark grey), and iNKT17 cells (GATA3$^+$, RORγt$^+$; light grey) of WT and Hobit × Blimp-1 KO mice. (H) The graph displays the frequency of iNKT17 (light grey), iNKT2 cells (grey), and iNKT$_{DN}$ (black) in the T-bet- iNKT cell population of the spleen of WT and Hobit × Blimp-1 KO mice. Plots in (A), (C), (E), and (G) are representative of graphs shown in (B), (D), (F), and (H). Graphs in (B) and (D) display data from two independent experiments with five to six mice per group. Graphs in (F) and (H) display data from two independent experiments with three mice per group. Symbols depict individual mice and error bars depict SEM.

Blimp-1 double deficient mice compared to WT mice (Supporting Information Figure S12A-C). In contrast, thymic populations of iNKT$_{CM}$ and iNKT$_{RM}$ cells were retained at WT levels in Hobit and Blimp-1 double deficient mice (Supporting Information Figure S12A–C). The combined impact of Hobit and Blimp-1 was required to drive iNKT$_{RM}$ formation at the expense of iNKT$_{CM}$ and iNKT$_{EM}$ formation, given that mice with single deficiencies in Hobit or Blimp-1 only had marginal phenotypes (Supporting Information Figure S13A-E). Underlining the impact of Hobit and Blimp-1 on the acquisition of a resident phenotype, we observed that the expression of the residency-associated molecules CD39, CD49a, CXCR6, and P2RX7 was decreased in the splenic iNKT cells of Hobit and Blimp-1 deficient mice compared to WT mice (Figure 6F and G). In contrast, the expression of TCF7 and CCR7 that associate with circulating T cells was increased in iNKT cells in the absence of Hobit and Blimp-1 (Figure 6F and G). Hobit

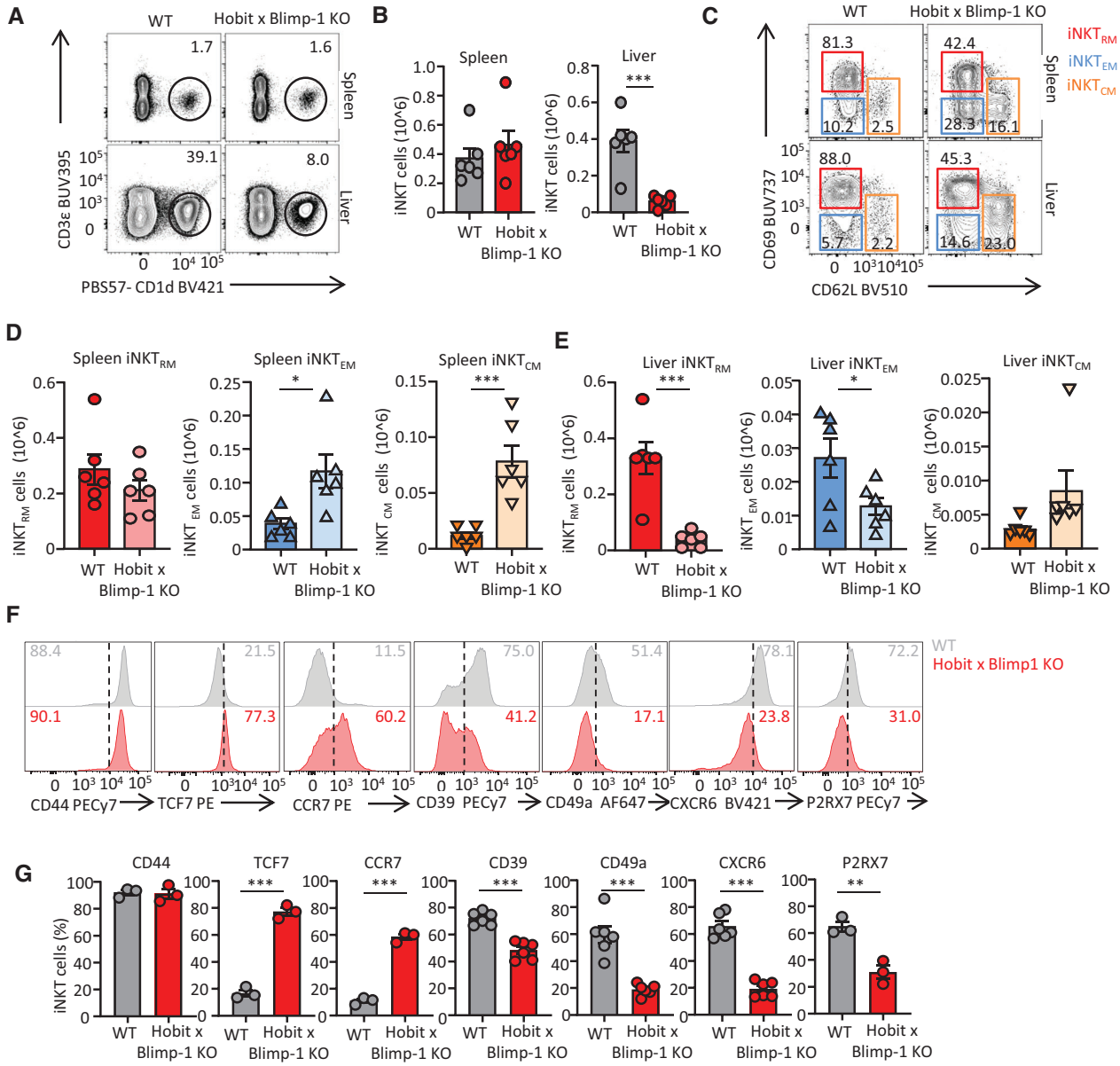

Figure 6. Hobit and Blimp-1 induce a resident phenotype in iNKT cells. The effect of Hobit and Blimp-1 on the phenotype of iNKT cells under steady-state conditions was analyzed in Hobit Reporter (WT) and in Hobit and Blimp-1 double deficient Hobit reporter mice using flow cytometry (Hobit × Blimp-1 KO). (A) Contour plots display the expression of TCR-β and the binding of PBS57-CD1d tetramers to identify iNKT cells in the spleen (upper panels) and liver (lower panels) of WT (left) and Hobit × Blimp-1 KO mice (right). (B) Graphs show the absolute number of splenic iNKT cells (left) and liver iNKT cells (right) in WT (grey) and Hobit × Blimp-1 KO mice (red). (C) Contour plots show the expression of CD69 and CD62L to identify $iNKT_{RM}$ (red), $iNKT_{EM}$ (blue), and $iNKT_{CM}$ (orange) in the spleen (upper panels) and liver (lower panels) of WT (left) and Hobit × Blimp-1 KO mice (right). (D) Graphs show the absolute number of $iNKT_{RM}$ (red), $iNKT_{EM}$ (blue), and $iNKT_{CM}$ (orange) in the spleen. (E) Graphs indicate the absolute number of $iNKT_{RM}$ (red), $iNKT_{EM}$ (blue), and $iNKT_{CM}$ (orange) in the liver of WT and Hobit × Blimp-1 KO mice. (F) Histograms depict the expression of CD44, TCF7, CCR7, CD39, CD49a, CXCR6, and P2RX7 in splenic iNKT cells of WT (grey) and Hobit × Blimp-1 KO mice (red). (G) Graphs display the percentage of CD44, TCF7, CCR7, CD39, CD49a, CXCR6, and P2RX7 expression in splenic iNKT cells of WT (grey) and Hobit × Blimp-1 KO mice (red). Plots in (A), (C), and (F) are representative of data shown in (B), (D), (E), and (G), respectively. Graphs in (B), (D), and (E) display data from six mice per group from two independent experiments and are representative of at least four independent experiments. Graphs in (G) display data from at least three to six mice per group and are representative of at least two independent experiments. Symbols represent individual mice, error bars SEM. Unpaired *T*-test, One-way ANOVA, $^{**}p < 0.005$, $^{***}p < 0.0005$.

and Blimp-1 did not completely block memory differentiation of iNKT cells, as evidenced by the retained expression of the memory-associated molecule CD44 in Hobit × Blimp-1 deficient mice compared to WT mice (Figure 6F and G).

To track the alternative differentiation path of the $iNKT_{RM}$ cells in the absence of Hobit and Blimp-1, we analyzed the expression of the tdTomato reporter in WT and Hobit × Blimp-1 deficient settings. Strikingly, $iNKT_{CM}$ in the spleen of Hobit and Blimp-1

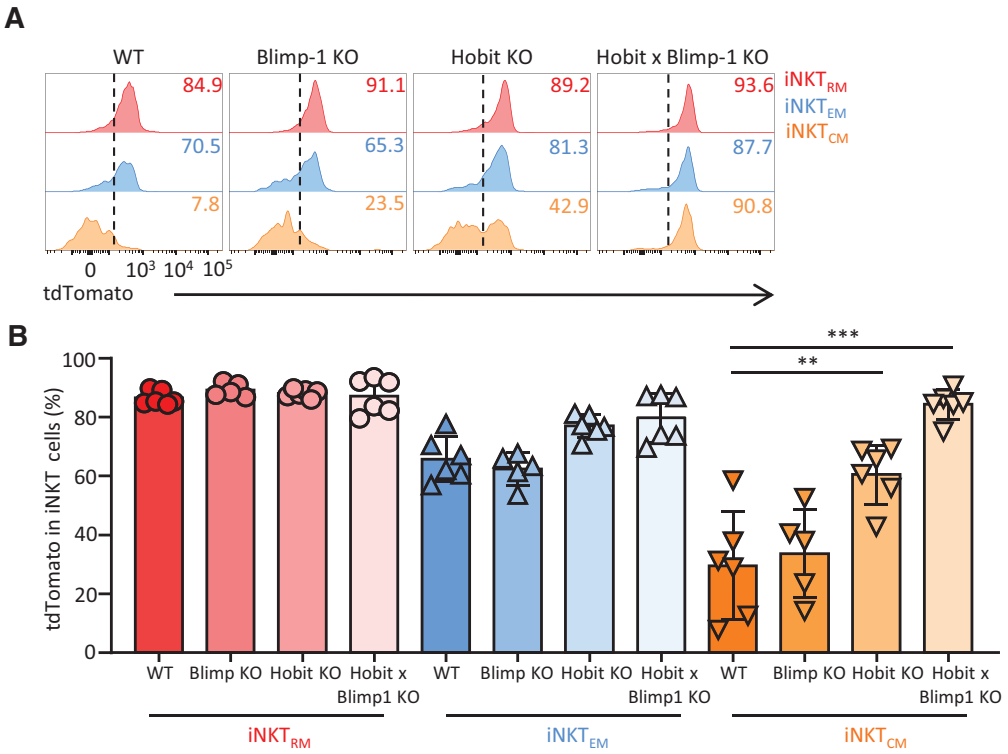

Figure 7. Hobit and Blimp-1 act at the branching point of NKT_{CM} and NKT_{RM} cells. The expression of the tdTomato reporter was analyzed in subsets of splenic iNKT cells of WT and Hobit and/or Blimp-1 deficient mice using flow cytometry. (A) Histograms display the expression of Hobit (tdTomato) in $iNKT_{RM}$ (red), $iNKT_{EM}$ (blue), and $iNKT_{CM}$ (orange) of the indicated mice. (B) The graph displays the percentage of tdTomato expression in $iNKT_{RM}$, $iNKT_{EM}$, and $iNKT_{CM}$ of the indicated mice. Plots in (A) are representative of data shown in (B). Graph in (B) displays data from two independent experiments with five to six mice per group and is representative for at least three independent experiments. Symbols represent individual mice, error bars SEM. One-way ANOVA, $^{**}p < 0.005$; $^{***}p < 0.0005$.

double deficient mice expressed tdTomato in contrast to $iNKT_{CM}$ of WT mice (Figure 7A and B). We did not observe differences in expression of tdTomato in $iNKT_{EM,}$ and $iNKT_{RM}$ in the spleen of WT and Hobit and/or Blimp-1 deficient mice (Figure 7A and B). These findings indicate that iNKT cells that would have developed in $iNKT_{RM}$ remained present in the absence of Hobit and Blimp-1 and were redirected into the alternative $iNKT_{CM}$ differentiation path. Therefore, Hobit and Blimp-1 appear to act at the branching point of $iNKT_{CM}$ and $iNKT_{RM}$ to instruct the differentiation of $iNKT_{CM}$ into $iNKT_{RM}$. To investigate whether the Hobit and Blimp-1-driven effects on iNKT cell differentiation persisted under competitive settings, we generated mixed bone marrow chimeras, containing WT and Hobit × Blimp-1 deficient compartments in a 1:1 ratio. WT and Hobit × Blimp-1 deficient iNKT cells were similarly present in the spleen of chimeric mice (Supporting Information Figure S14A and B). In contrast, Hobit × Blimp-1 deficient iNKT cells were much less prevalent within the liver compared to WT iNKT cells [Supplementary Figure S14A, B]. We observed the reduced formation of $iNKT_{RM}$ and increased formation of $iNKT_{EM}$ and $iNKT_{CM}$ in the Hobit × Blimp-1 deficient compartment compared to the WT compartment of the spleen (Supporting Information Figure S14C and D]. The expression of tdTomato was substantially elevated in the $iNKT_{CM}$ population of the Hobit × Blimp-1 deficient compartment compared to the WT compartment (Supporting Information Figure S14E and F), but WT and Hobit × Blimp-1 deficient $iNKT_{EM}$ and $iNKT_{RM}$ expressed tdTomato to a similar extent (Supporting Information Figure S14E and F). Thus, these findings support that the transcription factors Hobit and Blimp-1 instruct the transition of $iNKT_{CM}$ into $iNKT_{RM}$ cells.

We next questioned whether the impact of Hobit and Blimp-1 was observed in the separate iNKT1, iNKT2, and iNKT17 lineages. Comparison of splenic iNKT2 and iNKT17 lineages between WT and Hobit × Blimp-1 deficient mice did not reveal any impact on the expression of CD62L and CD69 (Figure 8A and B; Supporting Information Figure S15). In contrast, Hobit and Blimp-1 deficient iNKT1 cells displayed reduced expression of CD69 and increased expression of CD62L compared to WT iNKT1 cells in the spleen (Figure 8A and B; Supporting Information Figure S15). Interestingly, uncommitted iNKT cells lacking T-bet, RorγT, and GATA3 expression largely expressed CD62L and lacked CD69 expression (Figure 8A and B). This phenotype of the uncommitted iNKT cells was not impacted by Hobit and Blimp-1 (Figure 8A and B; Supporting Information Figure S15). These findings show that Hobit and Blimp-1 instruct the transition of $iNKT_{CM}$ into $iNKT_{RM}$ after commitment to the iNKT1 lineage. Thus, sequential programs of lineage commitment and residency operate in developing iNKT cells resulting in the Hobit and Blimp-1 independent

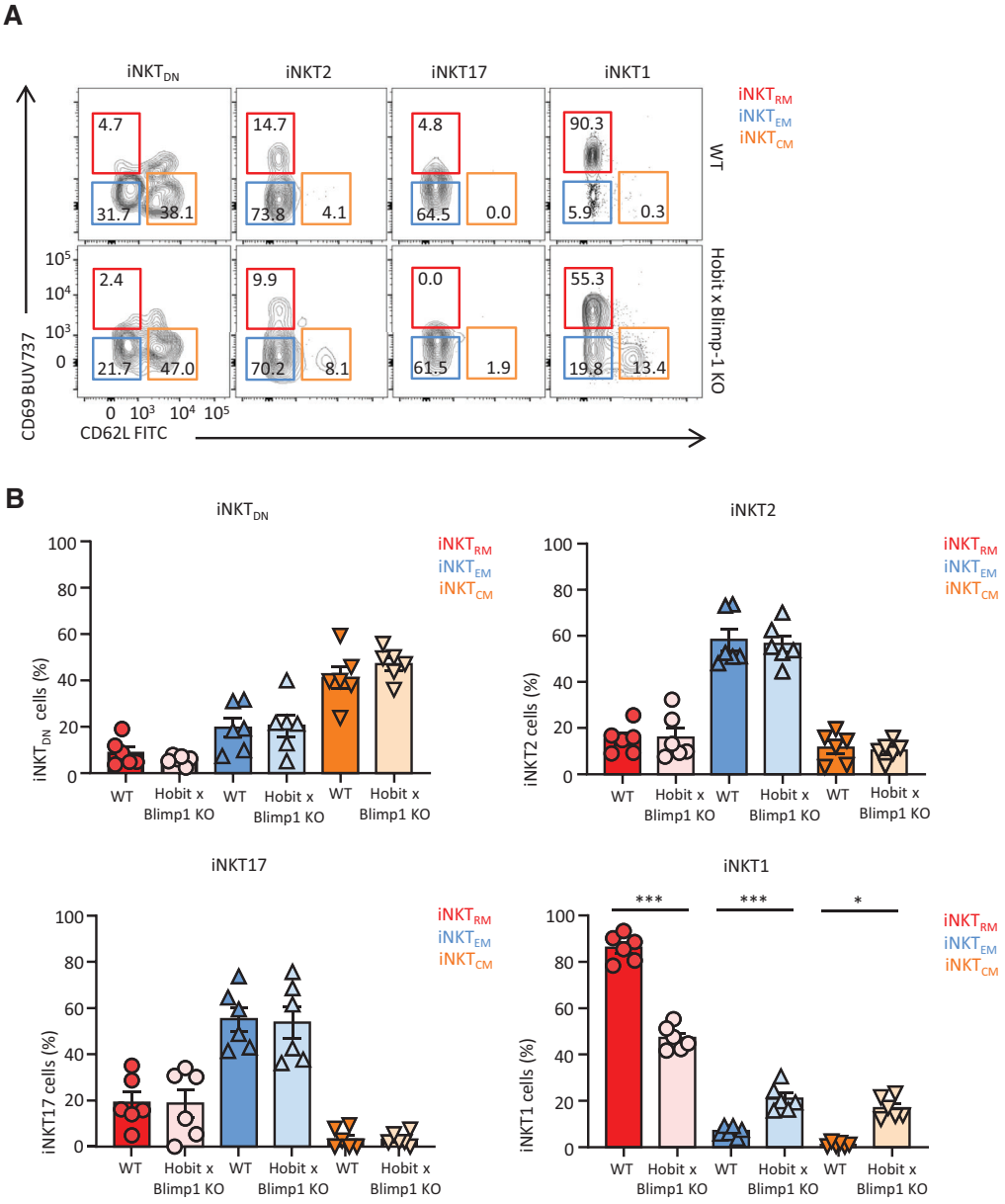

Figure 8. Hobit and Blimp-1 induce a resident phenotype after lineage commitment to iNKT1 cells. The impact of Hobit and Blimp-1 on the formation of resident-phenotype iNKT cells was analyzed separately in the distinct $iNKT_{DN}$, iNKT1, iNKT2, and iNKT17 lineages of the spleen using Hobit Reporter (WT) and Hobit and Blimp-1 double deficient Hobit reporter (Hobit × Blimp-1 KO) mice. (A) Contour plots display the expression of CD69 and CD62L in the indicated subsets of iNKT cells in WT (upper panels) and Hobit × Blimp-1 KO mice (lower panels). (B) Graphs display the frequency of $iNKT_{RM}$ (red), $iNKT_{EM}$ (blue), and $iNKT_{CM}$ (orange) within the indicated iNKT cell populations of the spleen in WT and Hobit × Blimp-1 KO mice. Plots in (A) are representative of data shown in (B). The graph in (B) displays pooled data from six mice per group from two independent experiments. Symbols represent individual mice, error bars SEM. One-way ANOVA, $^{**}p < 0.005$.

establishment of iNKT1, iNKT2, and iNKT17 lineages and the Hobit and Blimp-1 dependent differentiation into $iNKT_{CM}$, $iNKT_{EM}$, and $iNKT_{RM}$ cells.

Discussion

iNKT cells emerge from the thymus as fully developed memory T cells with the immediate potential to exert effector functions under steady-state conditions. The majority of iNKT cells eventually form resident memory populations that are permanently retained at peripheral sites. This important quality of tissue residency appears at odds with the early establishment during the thymic development of iNKT cells. Here, we have reported that thymic and peripheral iNKT cells largely identify as TRM-phenotype cells. In addition, minor, but significant, subsets of iNKT cells were identified that displayed TEM and TCM phenotypes consistent with circulating potential in a fraction of iNKT

cells. We have recently developed Hobit reporter/deleter mice that have enabled us to substantially improve the resolution of Hobit expression in iNKT cell subsets. Hobit was predominantly expressed in the $iNKT_{RM}$ fraction of the iNKT1, iNKT2, and iNKT17 lineages. Moreover, we found that Hobit together with the related transcription factor Blimp-1 instructed the acquisition of residency-associated molecules, but did not impact on lineage commitment of iNKT cells. These findings suggest that Hobit and Blimp-1 control final maturation steps resulting in the establishment of tissue-resident memory populations after the commitment of iNKT1, iNKT2, and iNKT17 lineages.

We have found that CD62L and CD69 expression define distinct subsets of peripheral iNKT cells that we have designated $iNKT_{CM}$, $iNKT_{EM}$, and $iNKT_{RM}$. The largely restricted expression of other molecules associated with tissue-residency such as CD39, CD49a, CXCR6, and P2RX7, and Hobit in $iNKT_{RM}$ and circulation-associated molecules such as TCF7 and CCR7 in $iNKT_{CM}$ and $iNKT_{EM}$ supports the classification into circulating and resident-phenotype iNKT cells. The $iNKT_{RM}$ subset is present within the iNKT1, iNKT2, and iNKT17 lineages, but appears much more prevalent within iNKT1 than in iNKT2 and iNKT17 lineages. These findings are consistent with earlier reports showing that the expression of CD69 is much more limited on iNKT2 and iNKT17 cells compared to iNKT1 cells [7,17]. CD69 directly antagonizes the tissue exit receptor S1PR1 [19], suggesting that CD69 may actively maintain the majority of iNKT1 cells as a resident population. However, CD69 does not appear solely responsible for the retention of iNKT1 in the spleen and thymus [17]. Alternative pathways such as through LFA-1/ICAM1 interactions likely contribute to the long-term persistence of iNKT1 in the tissues [7,9]. Despite the absence of CD69 expression on the majority of iNKT17 cells, a large proportion of these cells are maintained as tissue-resident cells [7]. The underlying mechanisms of the regulation of tissue residency in iNKT17 cells remain unclear. Thus, iNKT1, iNKT2, and iNKT17 lineages form heterogenic populations with respect to the regulation of tissue residency with a CD69-dependent mechanism dominating in the iNKT1 lineage, but not in the iNKT2 and iNKT17 lineages.

The differentiation of mature iNKT cells is initiated in the thymus and entails lineage specification into iNKT1, iNKT2, or iNKT17 cells and the establishment of tissue residency. The completion of these differentiation processes of splenic and liver iNKT cells appears to occur at peripheral sites rather than in the thymus. Although the thymus contains lineage-committed populations of iNKT1, iNKT2, and iNKT17, these subsets do not directly contribute to the seeding of the peripheral tissues. iNKT cells that have recently emigrated from the thymus do not yet express lineage-defining transcription factors such as T-bet and RorγT, suggesting that lineage commitment of iNKT cells is established in the periphery from uncommitted precursors [17]. Recent thymic emigrants of iNKT cells have been described within the $CD44^{high}NK1.1^{low}$ fraction [20] and more recently within the $CCR7^{+}$ fraction of peripheral iNKT cells [17]. iNKT cells employ the transcription factor KLF-2 and its downstream target S1PR1 to exit the thymus [17, 21], suggesting that $CCR7^{+}$ precursors emerge as $CD69^{-}$ iNKT cells. These recent thymic emigrants appear to overlap with the $CD69^{-}$ $iNKT_{CM}$ population that partially expresses CCR7. Our findings suggest that the establishment of tissue residency occurs downstream of lineage specification. Thus, it appears that the $CCR7^{+}$ recent thymic emigrants first diversify into iNKT1, iNKT2, and iNKT17 cells before they acquire a tissue-resident phenotype.

The differentiation of iNKT cells appears to be under the control of a hierarchical network of transcription factors. The broad complex, tramtrack, bric-a-brac-zinc finger transcription factor promyelocytic leukemia zinc finger (PLZF) acts as the master regulator of iNKT cells that drives memory formation of the lineage. In the absence of PLZF iNKT cells arrest in an immature $CD44^{low}CD62L^{high}$ naive-like stage and preferentially accumulate in the lymph nodes similar to conventional T cells [22,23]. In contrast, enforced expression of PLZF drives memory formation in conventional T cells [23,24]. The lineage-driving transcription factors Tbet and RorγT act downstream of PLZF to establish the iNKT1 and iNKT17 lineages, respectively [4, 25]. We have previously shown that the transcription factors Hobit and Blimp-1 collaborate to establish the transcriptional program of tissue-residency in lymphocyte lineages that include iNKT cells [8]. In this report, we have shown that Hobit and Blimp-1 did not impact the differentiation into iNKT1, iNKT2, and iNKT17 cells. In contrast, Hobit and Blimp-1 instructed the acquisition of the residency-associated molecules CD39, CD49a, CD69, CXCR6, and P2RX7 and impaired upregulation of molecules associated with migratory potentials such as CD62L, CCR7, and TCF7. These findings strongly support that Hobit and Blimp-1 drive the development of $iNKT_{RM}$ after lineage commitment of iNKT cells. The elevated expression of Hobit in the iNKT1 lineage compared to the iNKT2 and iNKT17 lineages may enforce stronger $iNKT_{RM}$ differentiation in this lineage. The inclusion of the Hobit promoter-driven reporter in Hobit and Blimp-1 deficient mice allowed us to visualize the alternative fate of $iNKT_{RM}$ in these mice. Strikingly, the Hobit promoter-driven reporter marked $iNKT_{CM}$ in Hobit and Blimp-1 deficient mice in contrast to WT mice. Therefore, our findings are consistent with an essential role for Hobit and Blimp-1 in the transition of $iNKT_{CM}$ into $iNKT_{RM}$ cells. This impact of Hobit and Blimp-1 on iNKT differentiation was not identical between the analyzed tissues. The requirement for Hobit and Blimp-1 in the formation of $iNKT_{RM}$ was more notable for populations in the thymus and liver than for those in the spleen. Potentially, the location of $iNKT_{RM}$ in the thymic epithelium or the vascular beds of the liver makes them more dependent on Hobit and Blimp-1. Despite the limited effect on $iNKT_{RM}$ numbers in the spleen, Hobit and Blimp-1 have a major impact on splenic iNKT cell differentiation. Previously, we have shown that splenic iNKT cells depend on Hobit and Blimp-1 to locate to the red pulp rather than the white pulp [8]. Moreover, in this report, we have shown that Hobit and Blimp-1 appeared to impair $iNKT_{CM}$ differentiation mostly in the spleen. In combination, these findings suggest that Hobit and Blimp-1 may enable iNKT1 cells to persist in peripheral rather than in lymphoid

tissues through the instruction of a T_{RM} phenotype instead of a T_{CM} phenotype. Importantly, the Hobit and Blimp-1 driven suppression of CD62L and CCR7 expression may limit access of iNKT1 cells to the spleen and lymph nodes. Thus, the differentiation of iNKT1 cells appears to involve sequential developmental stages of PLZF-driven memory formation, Tbet-driven lineage specification, and finally Hobit and Blimp-1-driven regulation of tissue residency.

Material and methods

Mice

C57BL/6JRj Ly5.2 and B6.SJL-Ptprc^{a}Pepc^b/BoyJ × C57BL6/JRj (CD45.1 × CD45.2) wild-type mice were either purchased from Janvier or bred in the animal facility of the Netherlands Cancer Institute (NKI). Hobit reporter ((B6-Tg(Zfp683-tdTomato-P2A-cre-P2A-DTR)) were generated as previously described [15]. Blimp-1 deficient, Hobit deficient [16], Hobit and Blimp-1 double-deficient mice, and *Blimp-1* ^{GFP} [26] were crossed on Hobit reporter mice to obtain lines of these mice with one Hobit reporter allele. Experimental mice were strictly matched by age (8–12 weeks) and gender. All of the mouse lines were maintained under SPF conditions at the mouse facility of the Netherlands Cancer Institute (NKI). Animal experiments were performed according to national and institutional guidelines.

Mixed bone marrow chimeras

Mixed bone marrow (BM) chimeras were generated by lethal irradiation (2 × 5Gy) of wild-type CD45.1 × CD45.2 bone marrow recipients, that were subsequently reconstituted with 2 × 10^7 bone marrow cells of donor mice. The recipient mice were intravenously injected with BM cells of Hobit Reporter (CD45.1$^+$) and Hobit and Blimp-1 double-deficient (CD45.2$^+$) mice in a 1:1 ratio. Cells of host and donor origin were identified using the congenic markers CD45.1 and CD45.2. Chimeric mice were analyzed 8–10 weeks after BM engraftment.

Cell preparation of murine tissues

Spleen, lymph nodes, thymus, and liver were isolated and ground over 70 μM nylon cell strainers (Corning) to obtain single-cell suspensions of lymphocytes from these organs in PBS containing 0.5% BSA. Liver lymphocytes were separated from the other cell fractions using 44% and 66% Percoll (GE Healthcare) density gradient centrifugation. The liver lymphocyte fraction was obtained from the interface of the 44% and 66% Percoll layers. Spleen and liver cell suspensions were incubated with erylysis buffer (155 mM NH_4Cl, 10 mM $KHCO_3$, and 1 mM EDTA) to remove contaminating red blood cells.

Diptheria toxin treatment

tdTomato$^+$ iNKT cells were deleted in vivo by injecting Hobit reporter mice intraperitoneally with 400 ng of diphtheria toxin (DT; Merck) in 200 μl PBS once a day for 4 consecutive days.

Antibodies and tetramers

The following anti-mouse monoclonal antibodies for flow cytometry were purchased from Thermo Fisher Scientific, BD Biosciences, or Biolegend: anti-TCRβ (H57-597, cat# 109224, 109206), anti-CD62L (MEL-14, cat# 746726, 104441, 17-0621-83), anti-CD69 (H1.2F3, cat# 564684, 612793), anti-CD122 (TM-β1, cat# 123207, 123216), anti-CD4 (GK1.5, cat# 11-0041-85), anti-CD8a (53-6.7, cat# 100712 anti-CD44 (IM7, cat# 11-0441-85, 103030, 56-0441-82), anti-NK1.1 (PK136, cat#564144), anti-Ly49C/F/I/H (14B11, cat# 108209), (90 cat#56-0381-82), anti-CD39 (24DM51, cat# 25-0391-82), anti-CD49a (Ha31/8, cat# 562113), anti-CXCR6 (SA051D1, cat# 151109), anti-P2 × 7 (1F11 cat# 94464), anti-CCR7 (4B12, cat# 562675) anti-TCF7 (S33-966, cat# 564217), anti-KI67 (B56, cat# 561277), anti-CD3Ɛ (145-2C11; cat# 563565), anti-T-bet (eBio4B10, cat# 12-5825-82), anti-RORγt (Q31-378, cat# 564722), GATA3 (L50-823, cat# 560068), anti-CD45.1 (A20, cat# 110714), and anti-CD45.2 (104, cat# 109822). Dead cells were excluded from our analysis using the LIVE/ DEAD Fixable Near-IR Dead Cell Stain kit (Invitrogen; L10119, cat# 2134021). To detect iNKT cells, tetramers of CD1d containing the α-GalCer derivative PBS57 (cat# 44870) were obtained from the Tetramer Core Facility of the US National Institutes of Health.

Flow cytometry

Flow cytometry was performed according to the guidelines [27]. Cells were stained with fluorochrome-conjugated antibodies in PBS supplemented with 0.5% FCS at 4°C for 30 min. For staining of intracellular transcription factors, the Foxp3/Transcription Factor Staining Buffer Set (eBioscience; 00-552-00) was used according to the instructions of the manufacturer. Labeling with CD1d-PBS57 tetramers (NIH tetramer core facility) was performed at 4°C for 30 min. Unbound antibodies and tetramers were removed by washing in PBS supplemented with 0.5% FCS. Samples were measured using an LSR Fortessa (BD Biosciences) and expression was analyzed using FlowJo V10 software (Tree Star).

Assessment of CRE recombinase activity at Blimp-1 locus

TCRβ$^+$ CD1d-PBS57$^+$ tdTomato$^-$, tdTomato$^+$ iNKT cells, and TCRβ$^+$ CD4$^+$ CD44$^-$ CD62L$^+$ Naive T cells were isolated from the spleen by flow cytometry-assisted cell sorting. Cell lysates of sorted naïve CD4 T cells, tdTomato$^-$, and tdTomato$^+$ iNKT

cells were obtained using lysis buffer (100 mM Tris-HCl, 5mM EDTA pH 8.0, 0.2% SDS, 200 mM NaCl, 200 μg/ml proteinase K (03115879001; Sigma–Aldrich). Genomic DNA (gDNA) was isolated from cell lysates using isopropanol extraction. The following forward primers were used for amplification of germline Blimp-1 (forward: 5'- GGCAAGATCAAGTATGAGTGC -3') and recombined Blimp-1 (forward: 5'- AGGTGTCTAGCCTTTGTATTTG-3'), in combination with a common reverse primer (reverse: 5'-TGAGTAGTCACAGAGTACCCA-3'). Amplification of gDNA was performed on a Verity 96 wells Fast Thermo Cycler (Applied Biosystems) using the DreamTaq Hot Start Green PCR Mastermix (Thermo Scientific, K9022). Samples were loaded onto a 2% agarose gel followed by gel electrophoresis at 100 V on a Mupid-One Sub-Cell GT from Biorad.

Statistics

Values are expressed as mean ± SEM as indicated. Differences between the two groups were assessed by the Student's *t*-test. Differences between more than two groups were assessed using one-way ANOVA followed by a Bonferroni post hoc test. A *p*-value of less than 0.05 was considered statistically significant ($*p < 0.05$; $**p < 0.005$; $***p < 0.0005$).

Acknowledgments: We would like to thank the members of the van Gisbergen Laboratory and the department of Hematopoiesis for fruitful discussions. N.A.M.K., K.P.J.M.v.G., and L.P.V. were supported by a fellowship of the Landsteiner Foundation of Blood Transfusion Research. R.S. was supported by Veni grant 016.186.116 from the Netherlands Organization for Scientific Research (NWO).

Conflict of interest: The authors declare no commercial or financial conflict of interest

Peer review: The peer review history for this article is available at https://publons.com/publon/10.1002/eji.202149360

Data availability statement: The data that support the findings of this study are available from the corresponding author upon reasonable request.

References

1 **Ma, C., Han, M., Heinrich, B., Fu, Q., Zhang, Q., Sandhu, M., Agdashian, D. et al.**, Gut microbiome-mediated bile acid metabolism regulates liver cancer via NKT cells. *Science*, 2018. **360**.

2 **Terabe, M. and Berzofsky, J. A.**, Tissue-Specific Roles of NKT Cells in Tumor Immunity. *Front Immunol*, 2018. **9**: 1838.

3 **Pellicci, D. G., Koay, H.-F. and Berzins, S. P.**, Thymic development of unconventional T cells: how NKT cells, MAIT cells and gammadelta T cells emerge. *Nat Rev Immunol*, 2020. **20**: 756–770.

4 **Lee, Y. J., Holzapfel, K. L., Zhu, J., Jameson, S. C. and Hogquist, K. A.**, Steady-state production of IL-4 modulates immunity in mouse strains and is determined by lineage diversity of iNKT cells. *Nat Immunol*, 2013. **14**: 1146–1154.

5 **Scanlon, S. T., Thomas, S. Y., Ferreira, C. M., Bai, Li, Krausz, T., Savage, P. B. and Bendelac, A.**, Airborne lipid antigens mobilize resident intravascular NKT cells to induce allergic airway inflammation. *J Exp Med*, 2011. **208**: 2113–2124.

6 **Geissmann, F., Cameron, T. O., Sidobre, S., Manlongat, N., Kronenberg, M., Briskin, M. J., Dustin, M. L. and Littman, D. R.**, Intravascular immune surveillance by CXCR6+ NKT cells patrolling liver sinusoids. *PLoS Biol*, 2005. **3**: e113.

7 **Salou, M., Legoux, F., Gilet, J., Darbois, A., Du Halgouet, A., Alonso, R., Richer, W. et al.**, A common transcriptomic program acquired in the thymus defines tissue residency of MAIT and NKT subsets. *J Exp Med*, 2019. **216**: 133–151.

8 **Mackay, L. K., Minnich, M., Kragten, N. A. M., Liao, Y., Nota, B., Seillet, C., Zaid, A. et al.**, Hobit and Blimp1 instruct a universal transcriptional program of tissue residency in lymphocytes. *Science*, 2016. **352**: 459–463.

9 **Thomas, S. Y., Scanlon, S. T., Griewank, K. G., Constantinides, M. G., Savage, A. K., Barr, K. A., Meng, F. et al.**, PLZF induces an intravascular surveillance program mediated by long-lived LFA-1-ICAM-1 interactions. *J Exp Med*, 2011. **208**: 1179–1188.

10 **Lynch, L., Michelet, X., Zhang, S., Brennan, P. J., Moseman, A., Lester, C., Besra, G. et al.**, Regulatory iNKT cells lack expression of the transcription factor PLZF and control the homeostasis of T(reg) cells and macrophages in adipose tissue. *Nat Immunol*, 2015. **16**: 85–95.

11 **Liu, Q. and Kim, C. H.**, Control of Tissue-Resident Invariant NKT Cells by Vitamin A Metabolites and P2×7-Mediated Cell Death. *J Immunol*, 1189–1197, 2019.

12 **Szabo, P. A., Miron, M. and Farber, D. L.**, Location, location, location: Tissue resident memory T cells in mice and humans. *Sci Immunol*, 2019. **4**.

13 **Berzins, S. P., Mcnab, F. W., Jones, C. M., Smyth, M. J. and Godfrey, D. I.**, Long-term retention of mature NK1.1+ NKT cells in the thymus. *J Immunol*, 2006. **176**: 4059–4065.

14 **Bovens, A. A., Wesselink, T. H., Behr, F. M., Kragten, N. A. M., Lier, R. A. W., Gisbergen, K. and Stark, R.**, Murine iNKT cells are depleted by liver damage via activation of P2RX7. *Eur J Immunol*, 2020. **50**: 1515–1524.

15 **Behr, F. M., Parga-Vidal, L., Kragten, N. A. M., Van Dam, T. J. P., Wesselink, T. H., Sheridan, B. S., Arens, R. et al.**, Tissue-resident memory CD8(+) T cells shape local and systemic secondary T cell responses. *Nat Immunol*, 2020. **21**: 1070–1081.

16 **van Gisbergen, K. P., Kragten, N. A. M., Hertoghs, K. M. L., Wensveen, F. M., Jonjic, S., Hamann, J., Nolte, M. A. and van Lier, R. A. W.**, Mouse Hobit is a homolog of the transcriptional repressor Blimp-1 that regulates NKT cell effector differentiation. *Nat Immunol*, 2012. **13**: 864–871.

17 **Wang, H. and Hogquist, K. A.**, CCR7 defines a precursor for murine iNKT cells in thymus and periphery. *Elife*, 2018. 7.

18 **Mcnab, F. W., Pellicci, D. G., Field, K., Besra, G., Smyth, M. J., Godfrey, D. I. and Berzins, S. P.**, Peripheral NK1.1 NKT cells are mature and functionally distinct from their thymic counterparts. *J Immunol*, 2007. **179**: 6630–6637.

19 **Shiow, L. R., Rosen, D. B., Brdičková, Nž, Xu, Y., An, J., Lanier, L. L., Cyster, J. G. and Matloubian, M.**, CD69 acts downstream of interferon-alpha/beta to

inhibit S1P1 and lymphocyte egress from lymphoid organs. *Nature*, 2006. **440**: 540–544.

20 **Benlagha, K., Kyin, T., Beavis, A., Teyton, L. and Bendelac, A.**, A thymic precursor to the NK T cell lineage. *Science*, 2002. **296**: 553–555.

21 **Allende, M. L., Zhou, D., Kalkofen, D. N., Benhamed, S., Tuymetova, G., Borowski, C., Bendelac, A. and Proia, R. L.**, S1P1 receptor expression regulates emergence of NKT cells in peripheral tissues. *FASEB J*, 2008. **22**: 307–315.

22 **Kovalovsky, D., Uche, O. U., Eladad, S., Hobbs, R. M., Yi, W., Alonzo, E., Chua, K. et al.**, The BTB-zinc finger transcriptional regulator PLZF controls the development of invariant natural killer T cell effector functions. *Nat Immunol*, 2008. **9**: 1055–1064.

23 **Savage, A. K., Constantinides, M. G., Han, J., Picard, D., Martin, E., Li, B., Lantz, O. and Bendelac, A.**, The transcription factor PLZF directs the effector program of the NKT cell lineage. *Immunity*, 2008. **29**: 391–403.

24 **Raberger, J., Schebesta, A., Sakaguchi, S., Boucheron, N., Blomberg, K. E. M., Berglöf, A., Kolbe, T. et al.**, The transcriptional regulator PLZF induces the development of CD44 high memory phenotype T cells. *Proc Natl Acad Sci U S A*, 2008. **105**: 17919–17924.

25 **Townsend, M. J., Weinmann, A. S., Matsuda, J. L., Salomon, R., Farnham, P. J., Biron, C. A., Gapin, L. and Glimcher, L. H.**, T-bet regulates the terminal maturation and homeostasis of NK and Valpha14i NKT cells. *Immunity*, 2004. **20**: 477–494.

26 **Kallies, A., Hasbold, J., Tarlinton, D. M., Dietrich, W., Corcoran, L. M., Hodgkin, P. D. and Nutt, S. L.**, Plasma cell ontogeny defined by quantitative changes in blimp-1 expression. *J Exp Med*, 2004. **200**: 967–977.

27 **Cossarizza, A., Chang, H.-D., Radbruch, A., Acs, A., Adam, D., Adam-Klages, S., Agace, W. W., Aghaeepour, N. et al.**, Guidelines for the use of flow cytometry and cell sorting in immunological studies (second edition). *Eur J Immunol*, 2019. **49**: 1457–1973.

Abbreviations: **iNKT**: invariant NK T cells · **PLZF**: promyelocytic leukemia zinc finger · **TCM**: central memory T cell · **TCR**: T cell receptor · **TEM**: effector memory T cell · **TRM**: tissue-resident memory T cell

Full correspondence: Natasja Kragten and Klaas van Gisbergen, Sanquin Blood Supply Foundation, Department of Hematopoeisis, Plesmanlaan 125, Amsterdam, 1006 CX, Netherlands
Email: n.kragten@sanquin.nl; k.vangisbergen@sanquin.nl

Received: 11/5/2021
Revised: 9/11/2021
Accepted: 8/12/2021
Accepted article online: 12/12/2021

